Electrical detection of electron-spin-echo envelope modulations in thin-film silicon solar cells

M. Fehr,[1,*] J. Behrends,[2] S. Haas,[3] B. Rech,[1] K. Lips,[1] and A. Schnegg[1]

[1]*Helmholtz-Zentrum Berlin für Materialien und Energie, Institut Silizium-Photovoltaik, Kekuléstr. 5, D-12489 Berlin, Germany*
[2]*Freie Universität Berlin, Fachbereich Physik, Arnimallee 14, D-14195 Berlin, Germany*
[3]*Forschungszentrum Jülich, Institut für Energie und Klimaforschung, Photovoltaik, D-52425 Jülich, Germany*

Electrically detected electron-spin-echo envelope modulations (ED-ESEEM) were employed to detect hyperfine interactions between nuclear spins and paramagnetic sites, determining spin-dependent transport processes in multilayer thin-film microcrystalline silicon solar cells. Electrical detection in combination with a modified Hahn-echo sequence was used to measure echo modulations induced by ^{29}Si, ^{31}P, and ^{1}H nuclei weakly coupled to electron spins of paramagnetic sites in the amorphous and microcrystalline solar cell layers. In the case of CE centers in the μc-Si:H i-layer, the absence of ^{1}H ESEEM modulations indicates that the adjacencies of CE centers are depleted from hydrogen atoms. On the basis of this result, we discuss several models for the microscopic origin of the CE center and conclusively assign those centers to coherent twin boundaries inside of crystalline grains in μc-Si:H.

The advance and successful commercialization of crystalline silicon (c-Si) solar cells demonstrates the practicality of large scale photovoltaic energy production. The high efficiencies that can be reached with wafer-based technologies, however, come along with the energy and cost intensive wafer production process. In contrast, thin film solar cells made from hydrogenated amorphous (a-Si:H) and microcrystalline silicon (μc-Si:H) can be deposited directly on inexpensive substrates like glass and are superior with regard to material consumption and cost effectiveness.[1–7] Despite these apparent benefits, thin-film silicon solar cells exhibit inferior electronic properties and efficiencies compared to their crystalline counterparts. It has been shown that the electron mobility in μc-Si:H is lower compared to polycrystalline and crystalline silicon materials.[8] There is evidence that the effective carrier mobility is reduced by trapping of delocalized charge carriers in shallow states of conduction band tails.[8,9] In order to improve the electron mobility, further understanding of the microscopic nature of these shallow states is necessary, which requires tailor made characterization tools capable of characterizing device limiting defects.

In μc-Si:H, the relevant defects are paramagnetic.[10–13] This renders electron paramagnetic resonance (EPR) the method of choice to unravel the microscopic defect structure and shed light on the influence of defect centers on charge-carrier transport mechanisms. In particular, hyperfine interactions (HFI) between the unpaired electron spin and nuclear spins in its vicinity constitute ultra sensitive probes of the defect wave function and the material composition in the vicinity of the defect. μc-Si:H is a mixed phase material with crystalline grains embedded in a hydrogenated amorphous matrix.[14] n-type μc-Si:H or intrinsic μc-Si:H under white light illumination show a prominent EPR signal with a g-value of $g = 1.9970$–1.9985 [denoted as conduction electron (CE) center].[10,11] Several possibilities for the microscopic origin of the CE center have been discussed in literature: (a) free electrons in the conduction band (CE resonance),[10] (b) interface defects at the boundary of amorphous and crystalline phases,[15] (c) electrons confined to an inversion layer

at the boundary of amorphous and crystalline phases of the material (Ref. 16) and (d) localized states due to internal twin grain boundaries inside of crystalline columns (Refs. 7 and 13). One way to distinguish between these models is to identify the microscopic structure of the CE center by determining how the unpaired electron spin is distributed over atoms in its vicinity. This requires knowledge about HFIs with nuclei in the first and second coordination shell accessible by EPR. However, the wave function of defects and impurities decays exponentially, and the vast majority of HFIs is small (<10 MHz) and usually not resolved in field-swept EPR spectra. Zhou *et al.*[17] investigated CE centers in μc-Si:H samples by electron-spin-echo envelope modulation (ESEEM) spectroscopy to detect small HFIs of the CE center with magnetic nuclei in their vicinity. They found that ESEEM spectra of CE centers lack contributions from hydrogen HFIs and therefore concluded that the vicinity of these centers is depleted from H atoms. This important finding implies that CE centers cannot be located at the interface between amorphous and crystalline phases of μc-Si:H due to the fact that the amorphous phase is H rich.[12] However, it remains unclear whether this assignment also holds true for CE centers in fully processed μc-Si:H solar cells, since Zhou *et al.*[17] studied highly crystalline and fairly conductive (dark conductivity @300 K: $\sigma_{RT} = 10^{-5}$ S/cm) powder samples with material properties being far from state-of-the-art thin-film solar cell materials (for a definition of state-of-the-art silicon materials see Ref. 2, Table 3.2, p. 55, Ref. 7, Chap. 3, and Ref. 18). However, ESEEM relies on conventional EPR and is therefore not applicable to fully-processed thin-film solar cells due to the low sensitivity of EPR. Very recently it was shown that this limit may be lifted by combining the sensitivity of electrical detection with advanced pulsed EPR detection schemes in an electrically detected (ED)-ESEEM experiment.[19] This progress essentially relies on the introduction of pulsed electrically detected magnetic resonance (pEDMR) techniques[20] approaching sensitivities down to single spin detection.[21] In the present work, we applied this method to study spin-dependent transport processes in a fully processed multilayer thin-film μc-Si:H solar cell with

TABLE I. PECVD deposition conditions for different layers of the investigated μc-Si:H solar cells. SC denotes the silane concentration in H$_2$; the dopant gas concentration is given as a percentage of the silane gas flow, P denotes the reactor power density, p_{dep} the chamber pressure during deposition, and T_s the substrate temperature. Sample laboratory reference: FZ-Jülich 05L-309.

Layer	SC [%]	Dopant gas [%]	P [W/cm^2]	p_{dep} [Torr]	T_s [°C]
p	0.3	0.5 (TMB)	0.28	10	200
i	0.8	–	0.25	10	150
n	9.1	1.0 (PH$_3$)	0.02	3	200

few electron spins (number of spins $\approx 10^4$). We show that this approach allows us to selectively investigate transport determining paramagnetic sites in the multilayer device.

Thin-film silicon p-i-n solar cells were deposited using 13.56 MHz plasma-enhanced chemical vapor deposition (PECVD) in the high radio-frequency power and high deposition pressure regime (for an overview of the PECVD deposition conditions see Table I).[5,22–25] The cells are deposited on Corning glass and consist of a layer stack with 150 nm ZnO:Al TCO, boron-doped p-μc-Si:H, 1-μm intrinsic μc-Si:H absorber, phosphorous-doped n-a-Si:H emitter, ZnO, and silver as a back contact. The total phosphorus and boron solid-phase concentration is estimated to be 1.5 at.% and 0.2 at.%, respectively. The hydrogen concentration in the thin n-a-Si:H layer is estimated to be 12(2) at.%.[26] The crystallinity[14] of the intrinsic μc-Si:H layer in the fully processed solar cell is 65% as determined by Raman spectroscopy. The hydrogen concentration in the intrinsic μc-Si:H layer is estimated to be 8(2) at.%.[27,28] Assuming that the crystalline phase contains negligible amounts of hydrogen, we can estimate the hydrogen content of the amorphous phase of the intrinsic μc-Si:H layer to be 22 at.%. All measurements were carried out on a commercially available BRUKER E580 spectrometer at 9.7 GHz in a dielectric ring resonator (ER 4118X-MD5) and using a laboratory-built current detection extension.[29] $\pi/2$-microwave pulses with a length of 16 ns ($S = 1/2$) were generated by using a 1 kW TWT microwave amplifier. The solar cell was operated in the reverse direction ($U_{bias} = -1.0$ V) and cooled to a temperature of 10 K by a He-flow cryostat, resulting in a photocurrent of 17 μA under illumination with a halogen lamp (50 mW/cm^2). The transient current response of the sample was recorded by a current amplifier and integrated from 3 μs to 8 μs for spin echo measurements to obtain a charge ΔQ. A detailed description of the experimental setup can be found in Ref. 29.

Figure 1 shows a field-swept pEDMR spectrum of the μc-Si:H solar cell recorded as a transient current change 3 μs after a 100 ns microwave π pulse. The spectrum exhibits two partly overlapping narrow signals with $g_e = 2.0045(5)$ and $g_{CE} = 1.9975(5)$, respectively and a 25 mT broad signal centered around $g_P = 2.003$. In a previous study, these signals have been assigned to spin-dependent transport between conduction band tail states (e) [$g_e = 2.0045(5)$] and neutral fourfold-coordinated P$_4^0$ donor atoms ($g_P = 2.003$) in the n-a-Si:H emitter layer.[30] The HFI between the P$_4^0$ donor electron and its host ^{31}P nucleus is on average 25 mT[31]
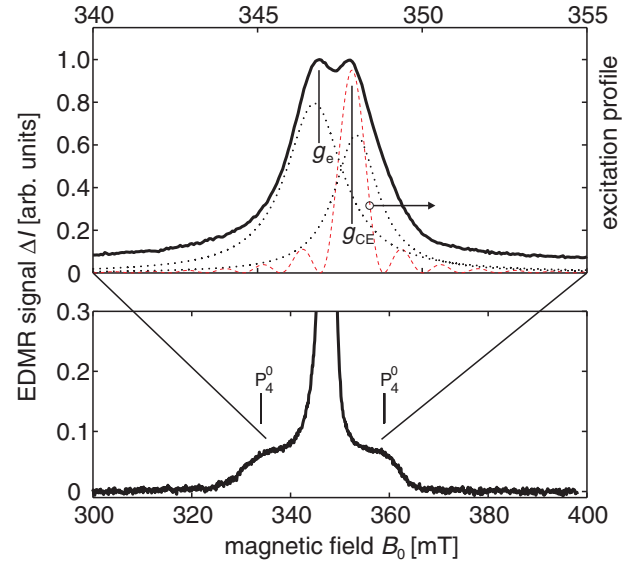

FIG. 1. (Color online) Field-swept pEDMR spectrum recorded by monitoring the transient current change (ΔI) 3 μs after a 100 ns π pulse. The pEDMR spectrum shows narrow resonances attributed to e and CE centers in addition to a broad resonance of P$_4^0$ donor states split by a large isotropic HFI. Deconvoluted pEDMR spectra are shown by dotted lines. ESEEM measurements are carried out at magnetic-field positions indicated by g_e and g_{CE}. The excitation profile of a 32 ns π-pulse is shown by the dashed line (red).

and therefore separates e center from P$_4^0$ donor transitions spectrally. The remaining signal has been assigned to hopping transport among CE centers [$g_{CE} = 1.9975(5)$] in the μc-Si:H absorber layer.[29] Since hopping transport can only occur between localized states in the mobility gap, CE centers observed here by EDMR cannot be attributed to free electrons in the conduction band (see above: model a).

In the following, we apply ED-ESEEM to investigate paramagnetic states in thin-film silicon solar cells, i.e., e centers in the n-type a-Si:H emitter and CE centers in the μc-Si:H absorber layer. From ED-ESEEM spectra, we estimate HFIs and discuss the microscopic origin of the investigated paramagnetic centers. ESEEM is based on a two-pulse sequence $\pi/2$-τ_1-π-τ_2 echo where coherences are refocused at $\tau_2 = \tau_1$ to generate a spin echo, whose amplitude is measured as a function of $\tau = \tau_1$. For electrical detection of the spin echo, the standard two-pulse ESEEM sequence is augmented with a $\pi/2$ readout pulse at the time of echo formation to transfer electron coherence to polarization [see Fig. 2(a)].[32] The observed EDMR hopping transport signals originate from two coupled $S = 1/2$ electron spins S_1 and S_2 and can be described within the coupled radical pair model.[33] As an example, we consider e center (S_1) and P$_4^0$ donor (S_2) electron-spin pairs. Transitions between CE states are described in a similar way and we assume that spin pairs are weakly coupled. Let us further assume that S_1 is coupled to a nuclear spin $I_1 = 1/2$ of, for now, arbitrary origin and that S_2 is solely coupled to its ^{31}P nuclear spin $I_2 = 1/2$. If the HFI between the excited electron spin (S_1) and I_1 is anisotropic, ESEEM is induced by the formation of coherence-transfer echoes.[34,35] Quantitatively, the two-pulse ED-ESEEM echo intensity for weakly coupled spin pairs as a function of τ under
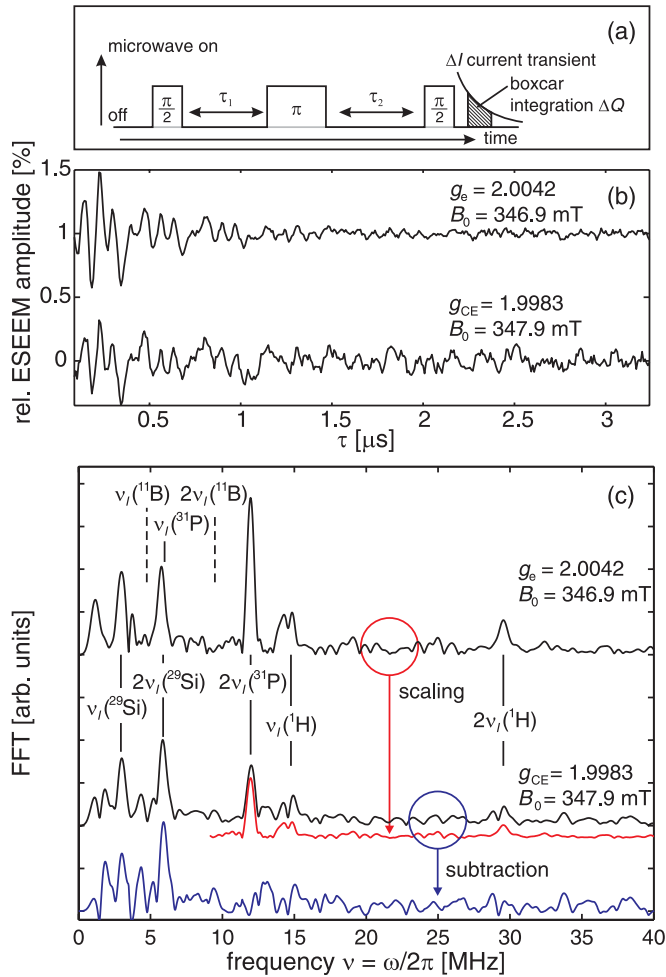
FIG. 2. (Color online) (a) Applied microwave pulse sequence together with a schematic current transient after the last read-out pulse, which serves as the observable in an ED-ESEEM experiment. (b) Electron-spin-echo envelope measured by simultaneously incrementing τ_1 and τ_2 and after division by a 9th-order polynomial fit. Upper trace: e centers ($g_e = 2.0042$), lower trace: CE centers ($g_{CE} = 1.9983$). (c) Magnitude FFT spectra of echo modulations in (b) normalized to $2\omega_I(^{29}$Si) modulation. Vertical lines indicate computed ω_I and $2\omega_I$ for given magnetic nuclear isotopes. The CE center spectrum contains residual contributions of the e center ESEEM spectrum. This part is subtracted from the CE center spectrum by, first, scaling the e center ESEEM spectrum (red spectrum) to the CE center spectrum using the $2\nu(^{31}$P) peak as a normalization point and, second, subtracting the scaled spectrum from the CE center trace. The true CE center ESEEM spectrum after subtraction is shown by the blue trace (lowest spectrum).

selective excitation of S_1 can be adapted from a calculation of spin-correlated radical pairs[36] and is given by

$$V_{2p}(\tau) = 1 - \frac{k}{4}(2 - 2\cos\omega_\alpha\tau - 2\cos\omega_\beta\tau$$
$$+ \cos\omega_+\tau + \cos\omega_-\tau) \qquad (1)$$

with nuclear frequencies of I_1: $\omega_{\alpha/\beta} = \sqrt{(\omega_{I_1} \pm \frac{A}{2})^2 + \frac{B^2}{4}}$, $\omega_\pm = \omega_\alpha \pm \omega_\beta$ and the modulation depth parameter $k = (\frac{B\omega_{I_1}}{\omega_\alpha\omega_\beta})^2$. For an axially symmetric HFI between S_1 and I_1 the secular and the pseudo-secular part can be expressed

as $A = A_{iso} + A_{dip}(3\cos^2\theta - 1)$ and $B = 3A_{dip}(\sin\theta\cos\theta)$, where A_{iso} and A_{dip} denote the isotropic and anisotropic HFI, respectively and θ indicates the angle between the external magnetic field vector and the axis connecting electron and nuclear spins.[37]

To record ESEEM, we incremented the delay times simultaneously $\tau_1 = \tau_2 = \tau$ and eliminated the unmodulated part of the echo envelope (approximate exponential decay time constant $T_D = 1.6$ μs) through division by a polynomial fit. The remaining modulated part of the echo envelope is shown in Fig. 2(b). Before fast-Fourier transformation (FFT), the time traces were apodized by a Kaiser 2π window to obtain a high side-band suppression and zero filled up to 4096 points.

The upper curve in Fig. 2(c) shows the FFT of the e center echo envelope. Several pronounced resonance peaks are observed at frequencies matching computed ω_I or $2\omega_I$ of ^{29}Si, ^{31}P, and ^{1}H nuclei, indicated by vertical lines in Fig. 2(c). According to Eq. (1), this means that each nuclear spin with nuclear frequencies $\omega_{\alpha/\beta} \approx \omega_I$ exhibits weak anisotropic and negligible isotropic HFI. Hence, the observed ESEEM pattern originates from a large number of distant matrix nuclei. Eq. (1) shows that in addition to modulations at the nuclear frequencies $\omega_{\alpha/\beta}$, the present ESEEM pulse sequence also gives rise to modulations at $\omega_+ \approx 2\omega_I$. Echo modulations at $\omega_- \approx 0$ are usually not observed since they overlap with the intense zero-frequency component of the time trace. The spectrum of e centers shows strong ^{31}P ESEEM since these centers are located in the a-Si:H emitter layer of the solar cell doped with a large concentration of phosphorous. Doping studies of a-Si:H showed that phosphorous atoms occur in threefold-coordinated (P$_3$) and fourfold-coordinated (P$_4$) atomic configurations, where only the latter acts as a dopant.[38] Although the experiment shows that the electron spins are coupled to ^{31}P nuclei, it is not immediately clear whether the ^{31}P nuclei are part of the diamagnetic (P$_3^0$) or paramagnetic (P$_4^0$) atomic configuration of P impurities. In both cases, the ^{31}P nuclear spin will interact with the electron spin of the e center (S_1) via HFI, also in case the paramagnetic P$_4^0$ is the actual spin-pair partner of the e center (special case $I_1 = I_2$). In the latter case, however, forbidden transitions involving a simultaneous flip of the electron and nuclear spin are shifted in energy relative to allowed S_1 transitions due to the large HFI between I and S_2 ($\approx$800 MHz). In this case, the condition for a simultaneous excitation of allowed and forbidden transitions, a prerequisite for the observation of ESEEM,[39] is not met due to a limited experimental excitation bandwidth ($\approx$100 MHz). We therefore attribute the ^{31}P nuclei observed by ESEEM to the P$_3^0$ configuration. This assignment is also supported by the fact that the present spin pairs observed by EDMR are weakly coupled, i.e., they exhibit a negligible electron-electron coupling. This indicates that the electron spins are separated by more than 3 nm, a value well beyond the detection radius of ESEEM ($\approx$8 Å).

CE centers were investigated under otherwise identical conditions by slightly tuning the magnetic field to excite centers with $g_{CE} = 1.9983$. The resulting ESEEM spectra are similar to those of e centers, but show a strong reduction of the $\omega_+(^{31}$P)/$\omega_+(^{29}$Si) intensity ratio [see lower curve in Fig. 2(c)] since CE centers are located in the undoped μc-Si:H absorber. The residual contribution of ^{31}P ESEEM is attributed to an

off-resonant excitation of e centers by the broad excitation profile of the microwave pulses and does not arise due to HFI between CE centers and ^{31}P nuclear spins. This is verified by a numerical simulation of the microwave pulse sequence excitation profile (see Fig. 1), which shows that the employed microwave pulses still excite a rather large fraction of the e center resonance. A quantitative simulation shows that the off-resonant e center contribution is only reduced by a factor of two when tuning the magnetic field to g_{CE} [see Fig. 2(c)]. We therefore conclude that the residual ^{31}P ESEEM does not originate from CE centers.

The same argumentation holds for ^{1}H ESEEM observed in the case of CE centers. The signal contributions at $\omega_I(^1$H) or $2\omega_I(^1$H) are reduced by about a factor of two as compared to e centers and can again be assigned to an off-resonant excitation of e centers. To recover the true ESEEM spectrum of CE centers free of contributions from off-resonant excitation of e centers, we first scale the e center ESEEM spectrum to the CE center spectrum using the $2\nu(^{31}$P) peak as a normalization point and, second, subtract the scaled spectrum from the CE center spectrum. The true CE center ESEEM spectrum after subtraction is shown by the blue trace (lowest spectrum) in Fig. 2(c). We see that within the signal-to-noise ratio, the CE centers do not exhibit ESEEM signal contributions at $\omega_I(^1$H) or $2\omega_I(^1$H). Hence, the density of distant hydrogen atoms around CE centers is significantly smaller than in the case of e centers. This observation now allows us to distinguish between microscopic models for the CE center introduced above (models b–d). Due to the lack of H coupling, the states must be located within H-free regions of the material. The crystalline columns present in μc-Si:H consist of grains of perfect crystal quality separated by grain boundaries.[40] In contrast to the amorphous matrix, the crystalline grains are expected to contain only a small quantity of H. The absence of ^{1}H-ESEEM in the case of CE centers is therefore a strong indication that these centers are not located in the amorphous phase or at the boundary between crystalline and amorphous phases since the amorphous phase contains H in large concentrations. This conclusion excludes models b and c where CE centers are attributed to interface defects or electrons confined to an inversion layer at the boundary of amorphous and crystalline

phases, since in the case of a planar interface the $\omega_I(^1$H) and $2\omega_I(^1$H) peak intensities should indicate a hydrogen density of about half the hydrogen content in the amorphous phase. Instead, the absence of ^{1}H ESEEM for CE centers suggests that these centers are located inside crystalline columns or grains (model d). However, in μc-Si:H, dislocations or point defects are absent in crystalline columns and grains.[40] The only important lattice distortions or crystal defects in crystalline grains are coherent twin boundaries with a high density (twin fault probability $\lambda = 0.1$).[40] Theoretical studies of the atomic and electronic structure of silicon twin grain boundaries revealed that they induce shallow localized electronic states.[41,42] The latter can be rationalized qualitatively by considering that coherent twin grain boundaries conserve the tetrahedral coordination of the lattice while the bond lengths and angles of Si atoms at the grain boundary are disturbed. This shifts the bonding and antibonding orbitals of Si-Si bonds, inducing the formation of electronic states at the band edges. A similar effect has been observed in the case of tilt boundaries in silicon bicrystals giving rise to conduction band tail states.[43] We therefore assign the microscopic origin of CE centers to localized conduction band tail states induced by twin grain boundaries. These centers are restricted to the crystalline phase of μc-Si:H.

In conclusion, we investigated e and CE centers in μc-Si:H thin-film solar cells by ED-ESEEM. Echo modulations arise due to highly-abundant matrix nuclei (^{29}Si, ^{31}P, and ^{1}H), which exhibit small HFIs and are therefore weakly coupled to paramagnetic sites. ESEEM of e centers in the a-Si:H emitter layer show a pronounced contribution of ^{31}P nuclei since the emitter layer is doped with a large amount of phosphorous. This contribution is strongly reduced in the case of CE centers since they are located in the undoped μc-Si:H absorber. In contrast to e centers, CE centers are not coupled to H atoms, and their vicinity is depleted from H. CE centers are assigned to localized states of twin grain boundaries in crystalline columns or grains of μc-Si:H.

*matthias.fehr@helmholtz-berlin.de

[1] A. Shah, P. Torres, R. Tscharner, N. Wyrsch, and H. Keppner, Science **285**, 692 (1999).

[2] R. E. I. Schropp and M. Zeman, *Amorphous and Microcrystalline Silicon Solar Cells: Modeling, Materials and Device Technology* (Springer, Berlin, New York, 1998).

[3] B. Rech and H. Wagner, Appl. Phys. A **69**, 155 (1999).

[4] H. Keppner, J. Meier, P. Torres, D. Fischer, and A. Shah, Appl. Phys. A **69**, 169 (1999).

[5] B. Rech, T. Roschek, T. Repmann, J. Müller, R. Schmitz, and W. Appenzeller, Thin Solid Films **427**, 157 (2003).

[6] J. Meier, U. Kroll, E. Vallat-Sauvain, J. Spitznagel, U. Graf, and A. Shah, Sol. Energy **77**, 983 (2004).

[7] A. Shah, *Thin-film Silicon Solar Cells* (EPFL Press, CRC Press, Lausanne, 2010).

[8] R. Carius, F. Finger, U. Backhausen, M. Luysberg, P. Hapke, L. Houben, M. Otte, and H. Overhof, Mater. Res. Soc. Symp. Proc. **467**, 283 (1997).

[9] R. Brüggemann, J. Appl. Phys. **92**, 2540 (2002).

[10] F. Finger, C. Malten, P. Hapke, R. Carius, R. Fluckiger, and H. Wagner, Philos. Mag. Lett. **70**, 247 (1994).

[11] J. Müller, F. Finger, R. Carius, and H. Wagner, Phys. Rev. B **60**, 11666 (1999).

[12] F. Finger, J. Müller, C. Malten, R. Carius, and H. Wagner, J. Non-Cryst. Solids **266–269**, 511 (2000).

[13] K. Lips, P. Kanschat, and W. Fuhs, Sol. Energy Mat. Sol. Cells **78**, 513 (2003).

[14] L. Houben, M. Luysberg, P. Hapke, R. Carius, F. Finger, and H. Wagner, Philos. Mag. A **77**, 1447 (1998).

[15] M. M. de Lima, P. C. Taylor, S. Morrison, A. LeGeune, and F. C. Marques, Phys. Rev. B **65**, 235324 (2002).

[16]J. P. Kleider, Y. M. Soro, R. Chouffot, A. S. Gudovskikh, P. R. i Cabarrocas, J. Damon-Lacoste, D. Eon, and P.-J. Ribeyron, J. Non-Cryst. Solids **354**, 2641 (2008).

[17]J. H. Zhou, S. Yamasaki, J. Isoya, K. Ikuta, M. Kondo, A. Matsuda, and K. Tanaka, Mater. Res. Soc. Symp. Proc. **452**, 821 (1997).

[18]Please note that in contrast to Schropp *et al.* (Ref. 2), device-quality μc-Si:H material giving the highest solar cell performance is usually found to be a mixture of a-Si:H and μc-Si:H (Raman crystallinity about 60%) and is generally not highly crystalline (Raman crystallinity about 90%) (see Ref. 28 and Sec. 3.3 in Ref. 7).

[19]F. Hoehne, J. Lu, A. R. Stegner, M. Stutzmann, M. S. Brandt, M. Rohrmüller, W. G. Schmidt, and U. Gerstmann, Phys. Rev. Lett. **106**, 196101 (2011).

[20]C. Boehme and K. Lips, Phys. Rev. B **68**, 245105 (2003).

[21]F. H. L. Koppens, K. C. Nowack, and L. M. K. Vandersypen, Phys. Rev. Lett. **100**, 236802 (2008).

[22]L. H. Guo, M. Kondo, M. Fukawa, K. Saitoh, and A. Matsuda, Jpn. J. Appl. Phys. **37**, L1116 (1998).

[23]T. Roschek, T. Repmann, J. Müller, B. Rech, and H. Wagner, J. Vac. Sci. Technol. A **20**, 492 (2002).

[24]S. Klein, T. Repmann, and T. Brammer, Sol. Energy **77**, 893 (2004).

[25]B. Rech, T. Repmann, M. N. van den Donker, M. Berginski, T. Kilper, J. Hupkes, S. Calnan, H. Stiebig, and S. Wieder, Thin Solid Films **511–512**, 548 (2006).

[26]T. F. Schulze, H. N. Beushausen, C. Leendertz, A. Dobrich, B. Rech, and L. Korte, Appl. Phys. Lett. **96**, 252102 (2010).

[27]Y. Mai, S. Klein, R. Carius, X. Geng, and F. Finger, Mater. Res. Soc. Symp. Proc. **862**, A23.2 (2005).

[28]Y. Mai, S. Klein, R. Carius, J. Wolff, A. Lambertz, F. Finger, and X. Geng, J. Appl. Phys. **97**, 114913 (2005).

[29]J. Behrends, A. Schnegg, M. Fehr, A. Lambertz, S. Haas, F. Finger, B. Rech, and K. Lips, Philos. Mag. **89**, 2655 (2009).

[30]J. Behrends, A. Schnegg, C. Boehme, S. Haas, H. Stiebig, F. Finger, B. Rech, and K. Lips, J. Non-Cryst. Solids **354**, 2411 (2008).

[31]M. Stutzmann and R. A. Street, Phys. Rev. Lett. **54**, 1836 (1985).

[32]H. Huebl, F. Hoehne, B. Grolik, A. R. Stegner, M. Stutzmann, and M. S. Brandt, Phys. Rev. Lett. **100**, 177602 (2008).

[33]R. Haberkorn and W. Dietz, Solid State Commun. **35**, 505 (1980).

[34]A. A. Maudsley, A. Wokaun, and R. R. Ernst, Chem. Phys. Lett. **55**, 9 (1978).

[35]A. Ponti and A. Schweiger, J. Chem. Phys. **102**, 5207 (1995).

[36]G. Zwanenburg and P. J. Hore, J. Magn. Reson. A **114**, 139 (1995).

[37]A. Schweiger and G. Jeschke, *Principles of Pulse Electron Paramagnetic Resonance* (Oxford University Press, Oxford, UK, New York, 2001).

[38]M. Stutzmann, D. K. Biegelsen, and R. A. Street, Phys. Rev. B **35**, 5666 (1987).

[39]A. Schweiger, C. Gemperle, and R. R. Ernst, J. Magn. Reson. **86**, 70 (1990).

[40]L. Houben, M. Luysberg, and R. Carius, Phys. Rev. B **67**, 045312 (2003).

[41]D. P. DiVincenzo, O. L. Alerhand, M. Schlüter, and J. W. Wilkins, Phys. Rev. Lett. **56**, 1925 (1986).

[42]M. Kohyama, R. Yamamoto, Y. Watanabe, Y. Ebata, and M. Kinoshita, J. Phys. C **21**, L695 (1988).

[43]J. Werner, W. Jantsch, and H. J. Queisser, Solid State Commun. **42**, 415 (1982).